


Kink Dynamics and Quantum Simulation of Supersymmetric Lattice Hamiltonians

Jiří Minář^{1,2}, Bart van Voorden¹, and Kareljan Schoutens^{1,2}¹*Institute for Theoretical Physics, University of Amsterdam, Science Park 904, 1098 XH Amsterdam, Netherlands*²*QuSoft, Science Park 123, 1098 XG Amsterdam, Netherlands* (Received 4 May 2020; revised 7 September 2021; accepted 7 January 2022; published 4 February 2022)

We propose a quantum simulation of a supersymmetric lattice model using atoms trapped in a 1D configuration and interacting through a Rydberg dressed potential. The elementary excitations in the model are kinks or (in a sector with one extra particle) their superpartners—the skinks. The two are connected by supersymmetry and display identical quantum dynamics. We provide an analytical description of the kink (skink) quench dynamics and propose a protocol to prepare and detect these excitations in the quantum simulator. We make a detailed analysis, based on numerical simulation, of the Rydberg atom simulator and show that it accurately tracks the dynamics of the supersymmetric model.

DOI: 10.1103/PhysRevLett.128.050504

Introduction.—Models of strongly interacting fermions are key to our understanding of condensed matter systems. At the same time, they are notoriously hard to track, even with sophisticated tools ranging from numerical approaches such as quantum Monte Carlo [1–3] and tensor networks [4,5] to application of gauge-gravity duality [6]. One strategy to make progress is to consider models with special symmetries. A nonstandard but intriguing choice is to consider *supersymmetry* as an explicit symmetry on the lattice [7–12] or as an emergent symmetry [13–15].

$\mathcal{N} = 2$ supersymmetry in a lattice model or a quantum field theory comes with a number of tools, such as the Witten index [16], which facilitate the analysis. Exploiting these tools unveils remarkable features such as extensive ground state degeneracies, a phenomenon dubbed superfrustration [17,18], which can lead to multicriticality [19].

Despite the supersymmetry, many hard questions remain, such as the nature of the quantum phases in higher spatial dimensions. Here a quantum simulator might provide ingenious insights to these questions. We make a step in this direction and propose such a simulator using arrays of neutral atoms trapped in optical potentials and dressed to their Rydberg state. This is motivated by the high versatility of these platforms [20–30] and by the fact that an off-resonant dressing [31–35] naturally implements the constrained dynamics inherent to the supersymmetric lattice model. Specifically, we consider a so-called M_1 model for spinless fermions on a 1D chain [8]. As a function of a parameter λ , this model interpolates between a trivial ($\lambda = 0$) and a quantum critical ($\lambda = 1$) phase, the latter connecting to superconformal field theory [8,36]. The value of the Witten index $W = 2$ indicates the existence of two supersymmetric vacua and points at kinks connecting these two vacua as elementary excitations. Furthermore, in a sector with one particle added, the excitations correspond to the *superpartners* of the kinks, which we call the skinks.

We propose a protocol for the (s)kink preparation and solve for their dynamics following a quench (we note a recent study of kink-antikink pair dynamics in a spin chain [37]). We show that it is identical in both cases and accurately reproduced by the quantum simulator. This is a direct consequence and a clear-cut sign of the underlying supersymmetry and we show how it can be revealed by a simple experimental probe based on monitoring single-site particle densities.

The M_1 model.—An $\mathcal{N} = 2$ supersymmetric lattice Hamiltonian for spinless fermions can be defined as

$$H_Q = \{Q, Q^\dagger\}, \quad (1)$$

where Q is the nilpotent supercharge, $Q^2 = 0$, and the brackets denote the anticommutator. The M_1 model [8] (on a bipartite graph) arises when $Q = \sum_i Q_i$ with $Q_i = (-1)^i \lambda_i c_i^\dagger P_{\langle i \rangle}$, where c_i are fermionic annihilation operators, $\{c_i, c_j\} = \{c_i^\dagger, c_j^\dagger\} = 0$, $\{c_i, c_j^\dagger\} = \delta_{ij}$, and $\lambda_i \in \mathbb{C}$. The M_1 model constraint, stipulating that fermions are not allowed to occupy nearest-neighbor sites $\langle ij \rangle$, is implemented via the projector $P_{\langle i \rangle} = \prod_{j \in \langle i \rangle} P_j$, with $P_j = 1 - n_j$, $n_j = c_j^\dagger c_j$. The Hamiltonian H_Q describes nearest-neighbor hoppings and local interactions; it preserves the number of particles, $[H_Q, \sum_i n_i] = 0$.

We now specialize to 1D and specify real $\vec{\lambda} = \{\lambda_1, \lambda_2, \dots, \lambda_L\}$, where L is the length of the chain, λ_i repeats every three sites in a pattern 11 λ and $\lambda \geq 0$. For this choice of staggering, the M_1 model is known to be integrable [38]. We refer to $\lambda = 0$ as “extreme staggering.”

Supersymmetric ground states.—Let us first consider periodic boundary conditions, $L = 3l$, $l \in \mathbb{N}$, and $\vec{\lambda} = (1, 1, \lambda, \dots, 1, 1, \lambda)$. In this case, there are two supersymmetric ground states with $E = 0$, each at 1/3 filling. At

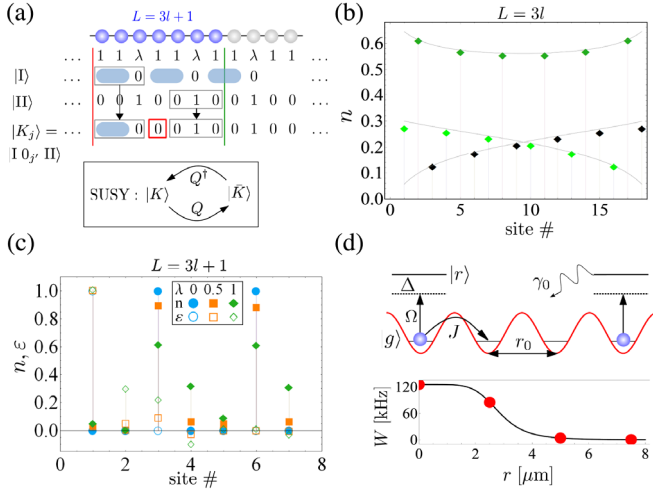


FIG. 1. (a) An infinite chain with staggering 11λ can accommodate two ground states $|I\rangle$, $|II\rangle$. The lowest energy states for an open chain of length $L = 3l + 1$ and l particles are kinks $|K_j\rangle$. A supercharge Q acting on a kink creates a particle at the kink location. The blue oval represents the triplet. (b) Particle densities in the ground state of an open chain, $L = 3l$, $\lambda = 1$ with an apparent \mathbb{Z}_3 pattern highlighted by the light green, dark green, and black data points. (c) Particle (filled symbols) and energy (empty symbols) densities of $|K_1\rangle$ for $\lambda = 0, 0.5, 1$ (blue circles, orange squares, green diamonds). (d) Scheme of the proposed realization. Atoms in their electronic ground state $|g\rangle$ tunnel in an optical lattice with spacing r_0 at rate J subject to dressing to a Rydberg state $|r\rangle$. Lower graph shows the dressed potential $W(r)$ for the $|84S\rangle$ state of ${}^6\text{Li}$ with $\Omega = 2\pi \times 10$ MHz, $\Omega/\Delta = 1/10$, $C_6 = 645$ GHz μm^6 .

extreme staggering, they are $|I\rangle \equiv |t_{1,2}0_3, \dots, t_{L-2,L-1}0_L\rangle$, $|II\rangle \equiv |0_10_21_3, \dots, 0_{L-2}0_{L-1}1_L\rangle$, where $t_{j,j+1} = 1/\sqrt{2}(c_j^\dagger + c_{j+1}^\dagger)|\text{vac}\rangle$ is the triplet state and $|\text{vac}\rangle$ is the fermionic vacuum, see Fig. 1(a). For an *open* chain of length $L = 3l$, the degeneracy is lifted and we have a single $E = 0$ ground state. Reference [38] analyzed the particle densities $\langle n_i \rangle$ in this ground state, perturbatively in $1/\lambda$. The same particle densities have been studied at the critical point $\lambda = 1$ by invoking conformal field theory, which provides closed form expressions for the associated scaling functions [36,39]. The corresponding particle densities constitute a direct experimental probe of the M_1 model as they follow a characteristic \mathbb{Z}_3 pattern indicated by the gray lines in Fig. 1(b) together with the data points (diamonds) for $l = 6$ (see Supplemental Material [39]).

Kinks at extreme staggering.—For an open chain of $L = 3l + 1$, there are no supersymmetric ground states. Instead, at extreme staggering the lowest energy states with l particles interpolate between the ground state configurations $|I\rangle$ and $|II\rangle$, with an empty site at position $i = 3j - 2$, with $j = 1, \dots, l + 1$. We write these “bare kink” states as $|K_j\rangle = |I_{[1,i-1]}0_i\Pi_{[i+1,L]}\rangle$, where $I_{[a,b]}$, $\Pi_{[a,b]}$ denote the part of the ground state configuration located between sites a

and b . They all have energy $E = 1$. The labels $j = 1(j = l + 1)$ correspond to the leftmost (rightmost) kink, see Fig. 1(a). Acting with the supercharge on the kink increases the number of particles by one creating the kink’s superpartner, the *skink*, $|\bar{K}_j\rangle \equiv Q|K_j\rangle = |I_{[1,i-1]}1_i\Pi_{[i+1,L]}\rangle$. Consequently, $Q^\dagger|\bar{K}_j\rangle = |K_j\rangle$ such that $|K_j\rangle$ and $|\bar{K}_j\rangle$ form doublets under supersymmetry, see Fig. 1(a) [77]. To characterize the kinks, we introduce a local energy density $h_i = \frac{1}{2}(\{Q, Q_i^\dagger\} + \{Q^\dagger, Q_i\})$ such that $H_Q = \sum_{i=1}^L h_i$.

Figure 1(c) shows the particle density $n = \langle n_i \rangle$ and energy density $\varepsilon = \langle h_i \rangle$ for the leftmost kink $|K_1\rangle$ for $\lambda = 0$ (blue data). The kink is clearly located at the left end of the chain with a corresponding peak in the energy density.

Kinks at general λ .—We claim that the notion of one-kink (and multikink) states is well defined also away from extreme staggering, when $0 < \lambda \leq 1$. To illustrate this, we present in the inset of Fig. 2(a) the spectrum of the system for $l = 4$. The energies become degenerate for $\lambda = 0$, taking odd positive values corresponding to the one-kink, three-kink, etc. states. The unavoided level crossings, characteristic for integrability, allow us to unambiguously characterize states as multikink states for all λ .

Figure 2(a) shows the low-lying part of the spectrum, which includes a band of $l + 1$ one-kink eigenstates $|v_k\rangle$ of energy E_k . We define a localized kink as [78]

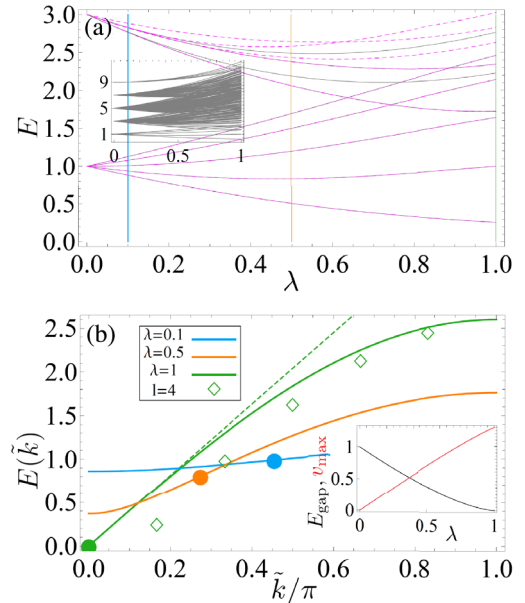


FIG. 2. (a) Spectrum (inset) and nine lowest eigenenergies for $l = 4$ in l (gray) and $l + 1$ (dashed magenta) particle-number sector of H_Q . (b) The dispersion Eq. (4) for $\lambda = 0.1, 0.5, 1$ (blue, orange, green). The filled circles correspond to the fastest mode \tilde{k} with v_{max} . The green diamonds denote the exact eigenenergies for $l = 4$ and $\lambda = 1$. The green dashed line is an eye guide depicting the linear dispersion at the origin. The inset shows the gap, i.e., the lowest energy (black) and v_{max} (red) vs λ .

$$|K_j\rangle = \sqrt{\frac{2}{l+2}} \sum_{k=1}^{l+1} \sin(\tilde{k}j) |v_k\rangle, \quad (2)$$

where $\tilde{k} = \pi k / (l+2)$.

In Fig. 1(c), the orange and green data points show the particle and energy densities in the state $|K_1\rangle$ obtained numerically using Eq. (2) for $\lambda = 0.5, 1$. We see that, even for $\lambda = 1$, the kink is well defined, with most of its energy localized at the kink position.

Kink dynamics.—We now proceed with the evaluation of the kink dynamics. We start from the leftmost kink $|K_1\rangle$ and consider overlap at time t with the rightmost kink, $o(t) \equiv \langle K_{l+1} | K_1(t) \rangle$, where $|K_1(t)\rangle = e^{-iH_0 t} |K_1\rangle$. It follows from Eq. (2) that

$$o(t) = \frac{2}{l+2} \sum_{k=1}^{l+1} \sin(\tilde{k}) \sin[\tilde{k}(l+1)] e^{-iE_k t}. \quad (3)$$

For simplicity, from now on we focus on the critical case $\lambda = 1$. In Fig. 3(a), we show $|o(t)|^2$ for $l = 4$ (solid blue line). At criticality, the fastest mode propagates with the Fermi velocity v_F , see the discussion after Eq. (4). This results in the onset of the overlap at $tv_F/l \approx 1$, with the maximum achieved for a later time, $tv_F/l \approx 1.75$.

Kink detection.—To make a connection with experimentally observable quantities, we construct an observable δn that detects the presence of a kink at the right end of the system, by requiring that $\langle K_i | \delta n | K_j \rangle \approx \delta_{i,l+1} \delta_{j,l+1}$. Taking $\delta n = \alpha(\lambda, l) [1 - \beta(\lambda, l)(n_{L-1} + n_{L+1})]$, we find $\alpha(0, l) = 1$ and $\beta(0, l) = 1$ for any l , and $\alpha(1, l) \approx 1.08$ and $\beta(1, l) \approx 1.09$ for $l = 3, 4$ [39]. The numerically obtained result for $\delta n(t)$ is shown as a blue dashed line in Fig. 3(a) and corresponds with good accuracy to $|o|^2$.

Kink preparation.—An important question is how the spatially localized kink $|K_1\rangle$ can be prepared in practice. To this end, we note that the kink site and its nearest neighbors remain approximately empty for all λ , cf. Fig. 1(c). We thus consider an adiabatic preparation of a ground state $|K'_1\rangle$ of the final Hamiltonian $H_f = H_Q + \mu(n_1 + n_2)$, where $\mu \rightarrow \infty$ ensures the kink condition on the first two sites. The initial Hamiltonian is chosen such that its ground state is a kink at extreme staggering $\lambda = 0$ (and similarly for skinks below), cf. Supplemental Material [39]. For $l = 4$, we find the fidelities $F \in [0.95, 1]$, where $F = |\langle K'_1 | K_1 \rangle|$, with the highest (lowest) value at extreme staggering (criticality). In Fig. 3(a), we show the numerically evaluated overlap $|o'|^2 = |\langle K_{l+1} | K'_1(t) \rangle|^2$ and the corresponding observable $\delta n'$ as solid (dashed) red lines. We find that, despite the limited fidelity of the initial state, $|o'|^2$ and $\delta n'$ agree well with $|o|^2$ and δn .

Skinks.—Supersymmetry guarantees that the one-skink energies [the lower dashed magenta lines in Fig. 2(a)] in the sector with $l+1$ particles are identical to the one-kink energies E_k . As a consequence, the quench dynamics

for the skinks is again given by Eq. (3). For the detection of $|\bar{K}_{l+1}\rangle$, we propose $\delta \bar{n} = -\bar{\alpha}(\lambda, l) [1 - \bar{\beta}(\lambda, l)(n_{L-2} + n_{L-1} + n_{L+1})]$, with $\bar{\alpha}(0, l) = 2$ and $\bar{\beta}(0, l) = 1$, and $\bar{\alpha}(1, l) \approx 1.46$ and $\bar{\beta}(1, l) \approx 0.98$ for $l = 3, 4$. For the preparation, we find that the ground state $|\bar{K}'_1\rangle$ of $H_f = H_Q + 3(-n_1 + n_2 - 0.5n_3)$ corresponds well to $|\bar{K}_1\rangle$ [39]. The $l = 4$ fidelities are $\bar{F} \in [0.93, 1]$ with $\bar{F} = |\langle \bar{K}'_1 | \bar{K}_1 \rangle|$.

Kink (skink) dynamics at large l .—Surprisingly, the kink arrival amplitude Eq. (3) is analytically tractable, for general λ , in the large- l limit. A key element for this is the continuum limit $E(\tilde{k})$ of the kink dispersion relation. Exploiting a relation between the M_1 model and the XYZ spin-1/2 chain [79], we have found [78]

$$E(\tilde{k}) = \frac{(3\lambda + s)^{3/2} \sqrt{1 - (1 - \frac{(-3\lambda+s)^3(\lambda+s)}{(-\lambda+s)(3\lambda+s)^3}) \cos^2(\frac{\tilde{k}}{2})}}{2\sqrt{2}\sqrt{\lambda+s}}, \quad (4)$$

where $s = \sqrt{8 + \lambda^2}$. In Fig. 2(b), we show the dispersion for $\lambda = 0.1, 0.5$, and 1. We denote by $v_{\max}(\lambda)$ the maximum

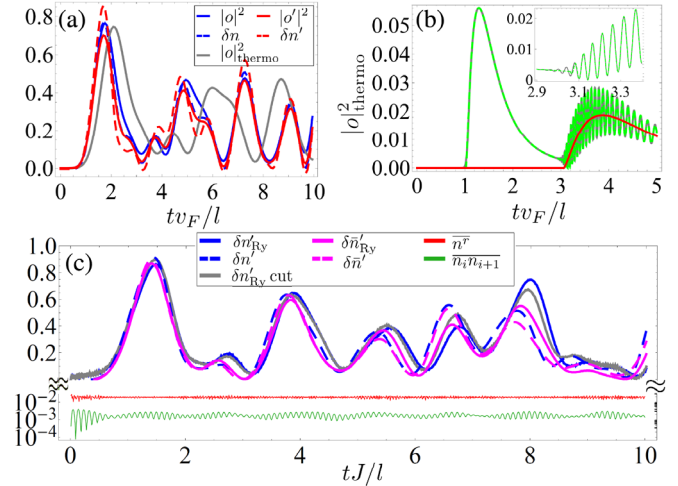


FIG. 3. (a) Time evolution of $|o(t)|^2$, Eq. (3) (solid lines) and δn (dashed lines) for a quench from the exact (blue) and reduced fidelity (red) kink state $|K_1\rangle$ for $l = 4$. The gray line corresponds to $|o(t)|^2$ evaluated with Eq. (4) for the eigenenergies. (b) Numerical evaluation [gray, Eq. (3)] and saddle point approximation [green dashed, red, Eq. (5)] of the overlap $|o(t)|^2$ for $l = 101$. The green (red) lines correspond to considering the first two (only the second) saddle points. The inset shows the onset of oscillations around $tv_F/l = 3$. (c) Quench dynamics for ten-site chain ($l = 3$), with initial states $|K'_1\rangle$ (blue) and $|\bar{K}'_1\rangle$ (magenta). Solid lines show dynamics under the full Hamiltonian H_{Ry} , whereas the gray curve is for a truncation of H_{Ry} , neglecting interactions beyond next-nearest neighbors. Dashed lines show dynamics under H_Q . The red line shows the average population in the Rydberg state $\bar{n} = 1/l \sum_i n'_i$, whereas the green line tracks the nearest-neighbor occupation of ground state atoms, $\bar{n}_i n_{i+1} = 1/l \sum_i n'_i n'_{i+1}$. Parameters as in Fig. 1(d).

value of the group velocity $v(\tilde{k}) = \partial_{\tilde{k}} E(\tilde{k})$. At criticality, $v_{\max}(\lambda = 1) = v_F = 3\sqrt{3}/4$, with v_F as the Fermi velocity. This gives real space velocity (since kinks hop three sites at a time) $3v_F = 9\sqrt{3}/4$, in agreement with [36].

In Fig. 3(a), the gray line shows the overlap Eq. (3) evaluated with the energies $E(\tilde{k})$ instead of E_k (blue line). The difference is a consequence of finite l , cf. the green diamonds vs green solid line in Fig. 2(b).

Using the dispersion $E(\tilde{k})$, we can evaluate the large- l limit of Eq. (3) in a saddle point approximation [39], giving

$$o(t) \approx \frac{2}{l+2} \sum_{s=1}^{\infty} \theta\left(\frac{v_{\max}t}{l+2} - (2s-1)\right) \sin(\tilde{k}_s)^2 \times e^{i[(2s-1)\pi k_s + E(\tilde{k}_s)t + i(5\pi/4)]} \sqrt{\frac{2\pi}{-E''(\tilde{k}_s)t}}, \quad (5)$$

where θ is the Heaviside step function, $k_s = E'^{-1}[(2s-1)\pi/t]$, $E' = \partial_{\tilde{k}} E(\tilde{k})$, $E'' = \partial_{\tilde{k}}^2 E(\tilde{k})$, and s labels the saddle point corresponding to the arrival times $t = (2s-1)(l+2)/v_{\max} \approx (2s-1)l/v_{\max}$, $s \in \mathbb{N}$, of the kink front (maximum velocity mode). At criticality, where $E(\tilde{k}) = 2v_F \sin(\tilde{k}/2)$, the saddle point expression takes a simple closed form [39].

In Fig. 3(b), we show an example of the dynamics for $l = 101$ evaluated using Eq. (3) (gray line) together with the prediction of Eq. (5) (green dashed line). We see a close to perfect agreement, with the inset showing the details around $tv_F/l = 3$, where the second saddle point $s = 2$ starts to generate the characteristic modulation of the overlap due to the interference of the kink front propagating at v_F incident on the right edge (after it has undergone one round-trip) and the kink tail. We note the frequency chirp of the modulation due to the nontrivial time dependence of \tilde{k}_s . Here we do not show the observable $\delta n(t)$, as for large l the Hamiltonian cannot be diagonalized exactly.

Experimental implementation.—We now discuss how H_Q can be engineered using Rydberg dressed atoms [40,41]; see Ref. [80] for an experimental realization of fermions hopping in an optical lattice and interacting through a Rydberg dressed potential.

We consider effectively two-level atoms with the ground and Rydberg states $|g\rangle$ and $|r\rangle$, where the ground state atoms experience an optical lattice potential and the atoms in a Rydberg state experience a repulsive van der Waals interaction described by

$$H_{\text{Ry}} = -J \sum_{i=1}^{L-1} (c_{i+1}^\dagger c_i + c_i^\dagger c_{i+1}) + \sum_{i=1}^L \mu_i n_i + \sum_{i=1}^L \Omega \sigma_i^x + \Delta n_i^r + \sum_{i>j=1}^{L-1} V_{ij} n_i^r n_j^r. \quad (6)$$

Here, $J > 0$ is the hopping amplitude, $\sigma^x = |r\rangle\langle g| + |g\rangle\langle r|$, $n^r = |r\rangle\langle r|$, and $V_{ij} = C_6/(r_0|i-j|)^6$ with C_6 as the van der Waals coefficient and r_0 as the lattice spacing. We consider a regime of large detuning $\Omega/\Delta \ll 1$, where the ground state atoms interact, up to order Ω^4 , through an effective flat potential $W(r = r_0|i-j|) = 2\Omega^4 V_{ij}/[\Delta^3(V_{ij} + 2\Delta)]$, cf. Fig. 1(d). To obtain the supersymmetric H_Q , the interaction and chemical potentials W and μ and the hopping J need to be tuned as follows.

For simplicity, we refer the discussion of general λ to the Supplemental Material [39] and focus on $\lambda = 1$. In this case, the chemical potential terms in H_Q become site-independent up to the boundary terms originating from $P_1 P_3$ and $P_{L-2} P_L$, which can be accounted for by setting $\mu_1 = \mu_L = J$.

Next, the M_1 model Hamiltonian forbids nearest-neighbor occupation while the potential terms are of the form $P_{i-1} P_{i+1}$, with no interactions beyond lattice distance 2. For this to be captured by the flat potential, we need $W(r_0)/W(2r_0) \gg 1$ and $W(2r_0)/W(3r_0) \gg 1$ with the maximum achieved in the limit $r_0 \rightarrow \infty$. However, to counteract experimental imperfections [39], one should reduce the duration of the simulation by maximizing the relevant energy scale, here $W(2r_0)$, which happens for $r_0 \rightarrow 0$, and one has to set $J = W(2r_0)$. This corresponds to the optimal approximation of H_Q using single dressing. Written explicitly,

$$JH_Q = -J \sum_{i=1}^{L-2} P_{i-1} (c_i^\dagger c_{i+1} + \text{H.c.}) P_{i+2} + J(n_1 + n_L) + J \sum_{i=1}^{L-2} n_i n_{i+2} \quad (7)$$

(up to global energy offset), see Supplemental Material [39] for details. Importantly, we also show in [39] that H_Q can be reached, in principle, with an arbitrary number of dressings with already a tenfold increase in $W(r_0)/W(2r_0)$ and $W(3r_0)/W(2r_0)$ for a double dressing with realistic parameters.

As a specific example, we consider the fermionic ${}^6\text{Li}$ dressed with the $|84S\rangle$ state with $C_6 = 645 \text{ GHz } \mu\text{m}^6$ [42,43] and lattice spacing $r_0 = 2.5 \mu\text{m}$. The resulting dressed potential is shown in Fig. 1(d). We get $W(2r_0) = J \approx 4 \text{ kHz}$, which for the optical lattice laser wavelength $\lambda = 2r_0 = 5 \mu\text{m}$ corresponds to lattice depth $\approx 5.5E_r$, with E_r being the recoil energy [44,81].

Figure 3(c) shows the quantum simulation of H_Q , where we compare the dynamics generated by the Rydberg Hamiltonian (6) with that of H_Q quenching from $|K'_1\rangle$ and $|\tilde{K}'_1\rangle$, see caption for details. We draw two main conclusions. First, the quantum simulator accurately tracks the dynamics set by the model Hamiltonian H_Q and, second, the dynamics in the l -particle sector (blue lines)

is highly similar to that in the $l + 1$ particle sector (magenta lines). The latter observation is direct evidence of the supersymmetry of H_Q .

Outlook.—We have proposed a realization of a supersymmetric lattice Hamiltonian H_Q based on atoms interacting through a Rydberg dressed potential [82,83]. Our results constitute a stepping stone to quantum simulations of supersymmetric lattice models in higher dimensions [18,84–87], which can require n -body, rather than two-body, interactions. In this context, it would be interesting to consider a scheme relying on coupling the Rydberg atoms with phonons [88] or to use cold molecules with permanent or electric-field-induced dipole moments, avoiding the need for off-resonant dressing [45–48]. Another interesting avenue is to exploit the mapping of the supersymmetric lattice Hamiltonians to spins [9,19,78,79], which would allow for simulations with platforms such as superconducting devices with n -body interactions [89,90].

We are very grateful to P. Fendley, I. Lesanovsky, Y. Miao, E. Ilievski, N. Chepiga, F. Schreck, K. van Druten, R. Spreuw, R. Gerritsma, T. Lahaye, B. Pasquiou, V. Barbé, and A. Urech for stimulating discussions. We also thank the anonymous referees for stimulating comments, in particular, about the symmetry aspects of the interaction potential that helped us to shape the Letter. This work is part of the Delta ITP consortium, a program of the Netherlands Organisation for Scientific Research (NWO) that is funded by the Dutch Ministry of Education, Culture and Science (OCW).

-
- [1] M. Suzuki, *Quantum Monte Carlo Methods in Condensed Matter Physics* (World Scientific, Singapore, 1993).
- [2] J. Gubernatis, N. Kawashima, and P. Werner, *Quantum Monte Carlo Methods* (Cambridge University Press, Cambridge, England, 2016).
- [3] F. Becca and S. Sorella, *Quantum Monte Carlo Approaches for Correlated Systems* (Cambridge University Press, Cambridge, England, 2017).
- [4] R. Orús, *Ann. Phys. (Amsterdam)* **349**, 117 (2014).
- [5] S. Montangero, *Introduction to Tensor Network Methods* (Springer, New York, 2018), 10.1007/978-3-030-01409-4.
- [6] J. Zaanen, Y. Liu, Y.-W. Sun, and K. Schalm, *Holographic Duality in Condensed Matter Physics* (Cambridge University Press, Cambridge, England, 2015).
- [7] H. Nicolai, *J. Phys. A* **9**, 1497 (1976).
- [8] P. Fendley, K. Schoutens, and J. de Boer, *Phys. Rev. Lett.* **90**, 120402 (2003).
- [9] P. Fendley, B. Nienhuis, and K. Schoutens, *J. Phys. A* **36**, 12399 (2003).
- [10] W. Fu, D. Gaiotto, J. Maldacena, and S. Sachdev, *Phys. Rev. D* **95**, 026009 (2017).
- [11] N. Sannomiya, H. Katsura, and Y. Nakayama, *Phys. Rev. D* **95**, 065001 (2017).
- [12] E. O’Brien and P. Fendley, *Phys. Rev. Lett.* **120**, 206403 (2018).
- [13] T. Grover, D. Sheng, and A. Vishwanath, *Science* **344**, 280 (2014).
- [14] L. Huijse, B. Bauer, and E. Berg, *Phys. Rev. Lett.* **114**, 090404 (2015).
- [15] Y. Yu and K. Yang, *Phys. Rev. Lett.* **105**, 150605 (2010).
- [16] E. Witten, *Nucl. Phys.* **B202**, 253 (1982).
- [17] H. van Eerten, *J. Math. Phys. (N.Y.)* **46**, 123302 (2005).
- [18] P. Fendley and K. Schoutens, *Phys. Rev. Lett.* **95**, 046403 (2005).
- [19] N. Chepiga, J. Minář, and K. Schoutens, *SciPost Phys.* **11**, 059 (2021).
- [20] A. Browaeys and T. Lahaye, *Nat. Phys.* **16**, 132 (2020).
- [21] C. Gross and I. Bloch, *Science* **357**, 995 (2017).
- [22] D. Barredo, S. De Léséleuc, V. Lienhard, T. Lahaye, and A. Browaeys, *Science* **354**, 1021 (2016).
- [23] M. Endres, H. Bernien, A. Keesling, H. Levine, E. R. Anschuetz, A. Krajenbrink, C. Senko, V. Vuletic, M. Greiner, and M. D. Lukin, *Science* **354**, 1024 (2016).
- [24] D. Barredo, V. Lienhard, S. De Leseleuc, T. Lahaye, and A. Browaeys, *Nature (London)* **561**, 79 (2018).
- [25] Y. Wang, S. Shevate, T. Wintermantel, M. Morgado, G. Lohead, and S. Whitlock, *npj Quantum Inf.* **6**, 54 (2020).
- [26] P. Schauß, J. Zeiher, T. Fukuhara, S. Hild, M. Cheneau, T. Macrì, T. Pohl, I. Bloch, and C. Groß, *Science* **347**, 1455 (2015).
- [27] H. Labuhn, D. Barredo, S. Ravets, S. De Léséleuc, T. Macrì, T. Lahaye, and A. Browaeys, *Nature (London)* **534**, 667 (2016).
- [28] H. Bernien, M. D. Lukin, H. Pichler, S. Choi, M. Greiner, V. Vuletić, A. Omran, H. Levine, S. Schwartz, A. Keesling, M. Endres, and A. S. Zibrov, *Nature (London)* **551**, 579 (2017).
- [29] S. de Léséleuc, V. Lienhard, P. Scholl, D. Barredo, S. Weber, N. Lang, H. P. Büchler, T. Lahaye, and A. Browaeys, *Science* **365**, 775 (2019).
- [30] S. Helmrich, A. Arias, G. Lohead, T. Wintermantel, M. Buchhold, S. Diehl, and S. Whitlock, *Nature (London)* **577**, 481 (2020).
- [31] J. B. Balewski, A. T. Krupp, A. Gaj, S. Hofferberth, R. Löw, and T. Pfau, *New J. Phys.* **16**, 063012 (2014).
- [32] Y.-Y. Jau, A. Hankin, T. Keating, I. Deutsch, and G. Biedermann, *Nat. Phys.* **12**, 71 (2016).
- [33] J. Zeiher, R. Van Bijnen, P. Schauß, S. Hild, J.-y. Choi, T. Pohl, I. Bloch, and C. Gross, *Nat. Phys.* **12**, 1095 (2016).
- [34] J. Zeiher, J.-y. Choi, A. Rubio-Abadal, T. Pohl, R. van Bijnen, I. Bloch, and C. Gross, *Phys. Rev. X* **7**, 041063 (2017).
- [35] A. Arias, G. Lohead, T. M. Wintermantel, S. Helmrich, and S. Whitlock, *Phys. Rev. Lett.* **122**, 053601 (2019).
- [36] L. Huijse, *J. Stat. Mech.* (2011) P04004.
- [37] A. Milsted, J. Liu, J. Preskill, and G. Vidal, *arXiv:2012.07243*.
- [38] P. Fendley and C. Hagendorf, *J. Stat. Mech.* (2011) P02014.
- [39] See Supplemental Material at <http://link.aps.org/supplemental/10.1103/PhysRevLett.128.050504> for (i) particle densities of the critical ground states, (ii) (s)kink profiles and observables, (iii) state preparation, (iv) saddle point approximation, and (v) details of the experimental implementation, which includes Refs. [36,40–76].

- [40] N. Henkel, R. Nath, and T. Pohl, *Phys. Rev. Lett.* **104**, 195302 (2010).
- [41] G. Pupillo, A. Micheli, M. Boninsegni, I. Lesanovsky, and P. Zoller, *Phys. Rev. Lett.* **104**, 223002 (2010).
- [42] N. Šibalić, J. D. Pritchard, C. S. Adams, and K. J. Weatherill, *Comput. Phys. Commun.* **220**, 319 (2017).
- [43] N. Šibalić, J. D. Pritchard, C. S. Adams, and K. J. Weatherill, Arc package, <https://arc-alkali-rydberg-calculator.readthedocs.io/en/latest/>.
- [44] M. Arzamasovs and B. Liu, *Eur. J. Phys.* **38**, 065405 (2017).
- [45] H. Büchler, A. Micheli, and P. Zoller, *Nat. Phys.* **3**, 726 (2007).
- [46] L. D. Carr, D. DeMille, R. V. Krems, and J. Ye, *New J. Phys.* **11**, 055049 (2009).
- [47] M. A. Baranov, M. Dalmonte, G. Pupillo, and P. Zoller, *Chem. Rev.* **112**, 5012 (2012).
- [48] N. Balakrishnan, *J. Chem. Phys.* **145**, 150901 (2016).
- [49] *Quantum Mechanics*, edited by A. Messiah (Dover Publications, New York, 1999).
- [50] S. Teufel, *Adiabatic Perturbation Theory in Quantum Dynamics* (Springer, New York, 2003).
- [51] T. Albash and D. A. Lidar, *Rev. Mod. Phys.* **90**, 015002 (2018).
- [52] J. E. Avron and A. Elgart, *Phys. Rev. A* **58**, 4300 (1998).
- [53] G. Rigolin and G. Ortiz, *Phys. Rev. A* **85**, 062111 (2012).
- [54] W. H. Press, S. A. Teukolsky, W. T. Vetterling, and B. P. Flannery, *Numerical Recipes 3rd Edition: The Art of Scientific Computing* (Cambridge University Press, Cambridge, England, 2007).
- [55] K. Agarwal, R. N. Bhatt, and S. L. Sondhi, *Phys. Rev. Lett.* **120**, 210604 (2018).
- [56] T. Macrì and T. Pohl, *Phys. Rev. A* **89**, 011402(R) (2014).
- [57] D. Jaksch and P. Zoller, *New J. Phys.* **5**, 56 (2003).
- [58] M. Aidelsburger, M. Atala, S. Nascimbène, S. Trotzky, Y.-A. Chen, and I. Bloch, *Phys. Rev. Lett.* **107**, 255301 (2011).
- [59] H. Miyake, G. A. Siviloglou, C. J. Kennedy, W. C. Burton, and W. Ketterle, *Phys. Rev. Lett.* **111**, 185302 (2013).
- [60] Z. Lan, J. c. v. Minář, E. Levi, W. Li, and I. Lesanovsky, *Phys. Rev. Lett.* **115**, 203001 (2015).
- [61] S. Wüster, C. Ates, A. Eisfeld, and J. Rost, *New J. Phys.* **13**, 073044 (2011).
- [62] E. A. Goldschmidt, T. Boulier, R. C. Brown, S. B. Koller, J. T. Young, A. V. Gorshkov, S. L. Rolston, and J. V. Porto, *Phys. Rev. Lett.* **116**, 113001 (2016).
- [63] T. Boulier, E. Magnan, C. Bracamontes, J. Maslek, E. A. Goldschmidt, J. T. Young, A. V. Gorshkov, S. L. Rolston, and J. V. Porto, *Phys. Rev. A* **96**, 053409 (2017).
- [64] J. T. Young, T. Boulier, E. Magnan, E. A. Goldschmidt, R. M. Wilson, S. L. Rolston, J. V. Porto, and A. V. Gorshkov, *Phys. Rev. A* **97**, 023424 (2018).
- [65] T. F. Gallagher, *Rydberg Atoms* (Cambridge University Press, Cambridge, England, 2005), Vol. 3.
- [66] S. Taie, R. Yamazaki, S. Sugawa, and Y. Takahashi, *Nat. Phys.* **8**, 825 (2012).
- [67] H. Ozawa, S. Taie, Y. Takasu, and Y. Takahashi, *Phys. Rev. Lett.* **121**, 225303 (2018).
- [68] S. Taie, E. Ibarra-García-Padilla, N. Nishizawa, Y. Takasu, Y. Kuno, H.-T. Wei, R. T. Scalettar, K. R. Hazzard, and Y. Takahashi, [arXiv:2010.07730](https://arxiv.org/abs/2010.07730).
- [69] I. Lesanovsky and H. Katsura, *Phys. Rev. A* **86**, 041601(R) (2012).
- [70] S. Paeckel, T. Köhler, A. Swoboda, S. R. Manmana, U. Schollwöck, and C. Hubig, *Ann. Phys. (Amsterdam)* **411**, 167998 (2019).
- [71] G. Carleo and M. Troyer, *Science* **355**, 602 (2017).
- [72] E. Zohar, J. I. Cirac, and B. Reznik, *Phys. Rev. Lett.* **109**, 125302 (2012).
- [73] D. Banerjee, M. Dalmonte, M. Müller, E. Rico, P. Stebler, U.-J. Wiese, and P. Zoller, *Phys. Rev. Lett.* **109**, 175302 (2012).
- [74] K. Kasamatsu, I. Ichinose, and T. Matsui, *Phys. Rev. Lett.* **111**, 115303 (2013).
- [75] J. F. Haase, L. Dellantonio, A. Celi, D. Paulson, A. Kan, K. Jansen, and C. A. Muschik, *Quantum* **5**, 393 (2021).
- [76] D. Paulson, L. Dellantonio, J. F. Haase, A. Celi, A. Kan, A. Jena, C. Kokail, R. van Bijnen, K. Jansen, P. Zoller *et al.*, *PRX Quantum* **2**, 030334 (2021).
- [77] T. Fokkema and K. Schoutens, *SciPost Phys.* **3**, 004 (2017).
- [78] J. Minář, Y. Miao, and K. Schoutens (to be published).
- [79] P. Fendley and C. Hagendorf, *J. Phys. A* **43**, 402004 (2010).
- [80] E. Guardado-Sanchez, B. M. Spar, P. Schauss, R. Belyansky, J. T. Young, P. Bienias, A. V. Gorshkov, T. Iadecola, and W. S. Bakr, *Phys. Rev. X* **11**, 021036 (2021).
- [81] In order to be well in the deep lattice limit where the tight-binding approximation is applicable, one might further reduce Ω/Δ . This would in turn reduce J and the achievable L_{\max} . To overcome this limitation, one could use a Raman-assisted hopping as we discuss in [39].
- [82] H. Weimer, L. Huijse, A. Gorshkov, G. Pupillo, P. Zoller, M. Lukin, and E. Demler, in *APS Division of Atomic, Molecular and Optical Physics Meeting Abstracts* (2012), <http://meetings.aps.org/link/BAPS.2012.DAMOP.T2.6>.
- [83] H. Weimer, L. Huijse, A. Gorshkov, G. Pupillo, P. Zoller, M. Lukin, and E. Demler, in *76. Annual Conference of the DPG and DPG Spring Meeting 2012* (2012), <https://www.dpg-verhandlungen.de/year/2012/conference/berlin/part/tt/session/19/contribution/10>.
- [84] L. Huijse, J. Halverson, P. Fendley, and K. Schoutens, *Phys. Rev. Lett.* **101**, 146406 (2008).
- [85] L. Huijse, D. Mehta, N. Moran, K. Schoutens, and J. Vala, *New J. Phys.* **14**, 073002 (2012).
- [86] D. Galanakis, C. L. Henley, and S. Papanikolaou, *Phys. Rev. B* **86**, 195105 (2012).
- [87] F. M. Surace, G. Giudici, and M. Dalmonte, *Quantum* **4**, 339 (2020).
- [88] F. M. Gabbetta, W. Li, F. Schmidt-Kaler, and I. Lesanovsky, *Phys. Rev. Lett.* **124**, 043402 (2020).
- [89] S. P. Pedersen, K. S. Christensen, and N. T. Zinner, *Phys. Rev. Research* **1**, 033123 (2019).
- [90] T. Roy, S. Hazra, S. Kundu, M. Chand, M. P. Patankar, and R. Vijay, *Phys. Rev. Applied* **14**, 014072 (2020).